Chapter 8

Durability of Building Joint Sealants

Christopher C. White,[1] Kar Tean Tan,[1] Donald L. Hunston,[1] and R. Sam Williams[2]

[1] National Institute of Standards and Technology, 100 Bureau Dr., MS 8615, Gaithersburg, MD 20899
[2] U. S. Department of Agriculture Forest Service, Forest Products Laboratory, Madison, WI USA 53726

Predicting the service life of building joint sealants exposed to service environments in less than real time has been a need of the sealant community for many decades. Despite extensive research efforts to design laboratory accelerated tests to duplicate the failure modes occurring in field exposures, little success has been achieved using conventional durability methodologies. In response to this urgent need, we have designed a laboratory-based test methodology that used a systematic approach to study, both independently and in combination, the major environmental factors that cause aging in building joint sealants. Changes in modulus, stiffness, and stress relaxation behavior were assessed. Field exposure was conducted in Gaithersburg, MD, using a thermally-driven exposure device with capabilities for monitoring changes in the sealant load and displacement. The results of both field and laboratory exposures are presented and discussed.

INTRODUCTION

Building joint sealants are filled elastomers that are an essential component of modern construction. They serve in weatherproofing of structures by preventing unwanted moisture intrusion and subsequent water damage. Over the past two decades, rapid technological advances and tremendous market growth in the building joint sealant industry have introduced a multitude of novel sealant products into the marketplace. In service, building joint sealants are exposed to various aging factors, including temperature, humidity, solar radiation, cyclic fatigue loading, etc. The interaction of these aging factors with sealants inevitably affects their properties and determines their long-term durability.[1-4] Hence, to reduce the risk of introducing poorly performing products into the marketplace, information on long-term performance of new products is needed. However, unlike existing building joint sealant products, new sealants lack long-term performance data. Various laboratory accelerated tests have been adopted to generate durability data, and to predict the long-term performance data in less than real time. However, building joint sealants have been reported to fail prematurely in the field even though they may have performed satisfactorily using these laboratory evaluations.

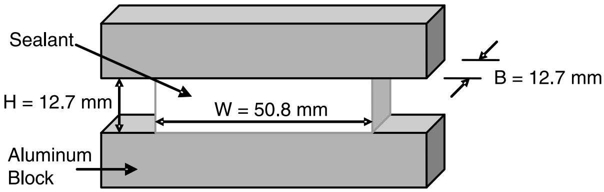

Figure 1—Schematic illustration of the test geometry used (not to scale).

Studies in the construction industry have shown a 50% failure rate within 10 years and a 95% failure rate within 20 years after installation.[5-7] What makes these failures particularly detrimental is that sealants are often used in areas where moisture-induced degradation is difficult to monitor and expensive to repair. Consequently, sealant failure is frequently detected only after considerable damage has occurred. In the housing market alone, premature failure of sealants and subsequent moisture intrusion damage is a significant contributor to the $65 billion–$80 billion spent annually on repair.[8] The aim of the present research, therefore, was to design a laboratory accelerated testing protocol that provides a platform for screening the relative importance of four different aging factors—temperature, humidity, radiation, and cyclic fatigue—acting independently and in combination on the degradation of building joint sealants. Since field exposure results have been designated as the standard of performance, outdoor field exposure was also carried out. This exposure was conducted in Gaithersburg, MD, using a polyvinyl chloride thermally-driven exposure device, which relies on changes in outdoor air temperature to induce cyclic fatigue deformation on sealant joints.

EXPERIMENTAL CONSIDERATIONS*

Materials and Specimen Preparation

A commercial sealant was provided by a member of a NIST/industry consortium, and formed into sealant joints conforming to the ASTM C719[9] specimen geometry shown in *Figure* 1. Specimens were prepared by extruding the sealant from a cartridge into a specimen cavity (50.8 mm x 12.7 mm x 12.7 mm) composed of aluminum supports (76.2 mm x 12.7 mm x 12.7 mm) on opposite sides with a polytetrafluoroethylene (PTFE) film on the back and PTFE spacers (12.7 mm x 12.7 mm) on each end. The specimens were cured in this fixture for 5 h at room temperature, and then removed from the fixture, keeping the PTFE spacers and the aluminum blocks intact. The samples were then allowed to cure for an additional three weeks as specified in the ASTM C719 test method.

EXPOSURE CONDITIONS AND CHARACTERIZATION

Laboratory Exposure and Characterization

Specimens were exposed to both field and laboratory accelerated conditions. The accelerated tests were conducted using a custom-made in-situ device with independent and precise control of temperature, humidity, radiation, and cyclic strain movement, and

*Certain commercial products or equipment are described in this paper in order to specify adequately the experimental procedure. In no case does such identification imply recommendation or endorsement by the National Institute of Standards and Technology, nor does it imply that it is necessarily the best available for the purpose.

built-in characterization functionality (see *Figure* 2). A full description of the hybrid device is documented elsewhere.[10] Temperature control was achieved via a precision temperature regulator; humidity control was accomplished via the proportional mixing of dry and saturated air. Highly uniform UV radiation was attained through the use of an integrating sphere-based weathering chamber, referred to as the Simulated Photodegradation via High Energy Radiant Exposure (SPHERE).[11] Six high intensity light sources were used in the SPHERE to produce a collimated and highly uniform ultraviolet flux of approximately 480 W/m^2. A computer-controlled stepper motor and a precision transmission system were used to provide precise movement control that imposed mechanical deformations on the sealant specimens. There was a total of eight specimen holders, each of which was attached to a hermetically sealed load cell (Model SSM-AJ-250, Interface, Scottsdale, AZ) with a capacity of ± 113.4 kg. To precisely measure device movement, two linear variable differential transformers (LVDT) (Model HSD-750, Macro Sensors, Pennsauken, NJ) with a deflection range of ± 6.35 mm were used.

During the exposure, half of the specimens were subjected to cyclic fatigue loading while the other half remained unloaded to provide a comparison. The fatigue deformation cycle involved varying the tensile strain between 25% and 50%. A total of 1460 cycles were imposed on the specimens (38 min/cycle). Prior to and after the exposure experiment, a characterization test was run, which consisted of two loading-unloading

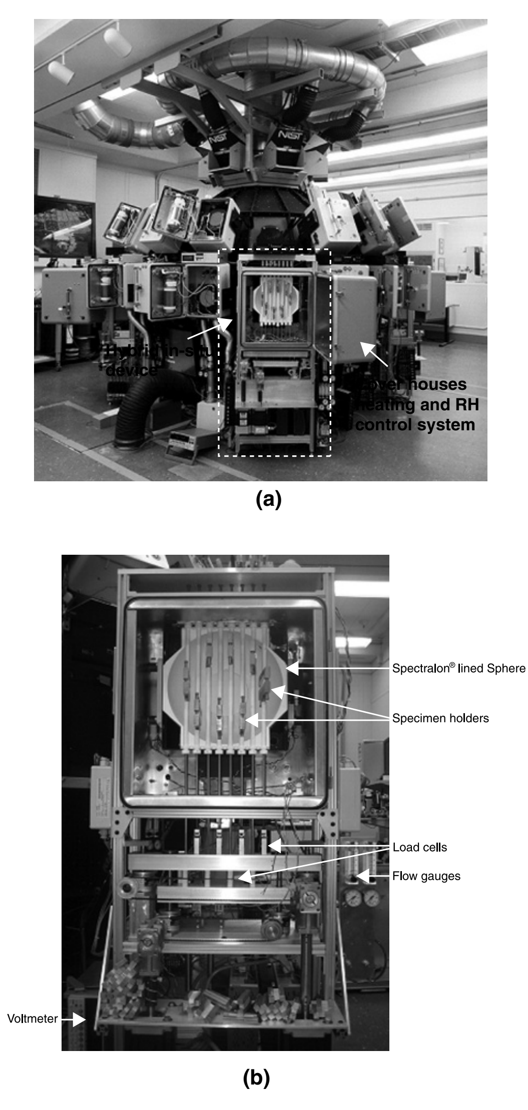

Figure 2—(a) An integrating sphere-based weathering chamber, referred to as the Simulated Photodegradation via High Energy Radiant Exposure (SPHERE), and (b) an in-situ device.

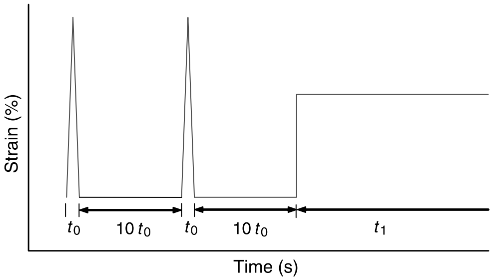

Figure 3—Strain history used for Mullins cycles and stress relaxation tests.

cycles (0% to 25% strain) and one stress relaxation measurement at 15% strain. After characterization, the specimens were allowed to recover before starting the fatigue cycling. The loading and unloading during characterization were performed at 2 cm/min which meant that the specimen was under load for a time period denoted as t_0. The time under load in the stress relaxation test was denoted as t_1. To ensure that the viscoelastic recovery from one loading was complete before the next loading was initiated, the specimen was allowed to rest for $10t_0$ or $10t_1$ between loadings (*Figure* 3). For these tests, the values for t_0 and t_1 were 20 s and 3 h, respectively. The motivation for the two loading-unloading cycles was to see if any Mullins Effect was present and to mitigate any Mullins Effect in the subsequent stress relaxation test. This Mullins Effect is a phenomenon observed in filled elastomers: the stress at a given strain is higher the first time the specimen is deformed than it is for subsequent deformations. As long as the maximum strain achieved during the first deformation is not exceeded, all subsequent loadings follow the same stress-strain curve. As a result, it is common to pre-strain a sample to high values so that the results are reproducible in subsequent testing.

For the stress relaxation measurements, specimens were loaded rapidly at 100 cm/min up to 15% strain and held at that value while load was monitored as a function of time. The time required to load a specimen was less than 1 s and the first data point was not taken until after 10 s to avoid transient effects associated with uploading. An apparent modulus, E_a, was calculated using a relationship based on the statistical theory of rubber-like elasticity[12-14]:

$$E_a(t,\lambda) = \frac{3L(t)}{WB(\lambda - \lambda^{-2})} \tag{1}$$

where W and B are the width and breadth of the sealant (see *Figure* 1), L is the load, t is the time, and λ is the extension ratio, which is given by:

$$\lambda = 1 + \frac{\Delta}{H} \tag{2}$$

where Δ is the cross-head displacement. Equation (1) assumes that the sealant is incompressible, which should be a good assumption for elastomers.

To examine the change in the specimen produced by exposure, the apparent modulus, E_a, from the characterizations before and after were compared. This was done by calculating the fractional change in apparent modulus, F. If exposure time is designated as t_e, then F is given by:

$$F = \frac{E_a(\text{at } t_e = 1\text{ month})}{E_a(\text{at } t_e = 0)} \tag{3}$$

A second way to monitor the changes during exposure was to calculate stiffness index based on loading curve in each cycle of the fatigue deformation experiment. This stiffness index was given by the slope of the linear regression curve fit to a plot of the voltage output for a load cell versus the voltage output for a LVDT. This produced 1460 points over the one month period. Unlike the stress relaxation experiments in which changes before and after exposure were only obtained, the use of stiffness index offered the advantage of monitoring changes during exposure. Squared correlation coefficients, r^2, for fitted curves were also obtained to measure goodness-of-fit of linear regression, and hence the reliability of the indexes. A custom-written LabVIEW (National Instruments, Columbia, MD) program was developed for signal generation, analysis, and data acquisition. More information can be found elsewhere in this literature.[10]

In addition to the presence or absence of fatigue deformation cycle during exposure, specimens were subjected to one of four different environments involving combinations of temperature and RH, i.e., (a) 30°C and 0% RH, (b) 30°C and 80% RH, (c) 60°C and 0% RH, and (d) 60°C and 80% RH. In this chapter, 60°C will hereafter be denoted as "hot," and 30°C as "cold." Also, 80% RH will hereafter be denoted at "wet," and 0% RH as "dry." As a result, there were eight different exposure conditions for the sealant material, and with four replicates of each, a total of 32 specimens were examined in each test.

Field Exposure and Characterization

Field exposure was performed in Gaithersburg, using custom-made *thermally* driven outdoor exposure engines, as shown in *Figure* 4. Each engine was composed of a moving frame and a fixed support frame. The moving frame consisted of two 101.6 mm diameter polyvinyl chloride (PVC) pipes (Schedule 40), a stainless steel crosspiece, six stainless steel rods, and six specimen holders; while the fixed support frame was comprised of a wood support frame, and a fixed stainless steel crosspiece. The strain on the sealant samples was generated by thermal changes in the exposure environment combined with the relative difference in the coefficient of thermal expansion between the PVC pipe and the end grain wood frames. A full description of the devices is reported elsewhere.[15] Specimens were placed into the device at a time when the temperature was approximately 13°C (55°F), so they were under no load at that temperature. At high temperatures PVC pipes expand, causing the specimens to be loaded in tension; conversely, the specimens are loaded in compression when the pipes contract at low temperatures, as shown schematically in *Figure* 4b and c. Consequently, the engines are also known as "winter/compression" or "summer/tension" engines. The engines were mounted facing south towards the equator at an angle of 90° from the horizontal plane.

To monitor the force on each specimen, each specimen holder was attached to a hermetically sealed load cell (Model SSM-AJ-250, Interface, Scottsdale, AZ) attached with a capacity of ± 113.4 kg. The displacement was monitored with LVDTs (Model HSD-750, Macro Sensors, Pennsauken, NJ) with a deflection range of ± 6.35 mm. The LVDTs were bolted between both fixed and moving stainless steel crosspieces. These electromechanical transducers were instrumented to monitor continuously forces and deflections. Also, each engine was attached to a series of six thermocouples to record the temperatures of PVC pipes. Data from load cells, LVDTs, and thermocouples were directly fed into a Keithley 2701 Ethernet-based Data Acquisition System (Keithley Instruments,

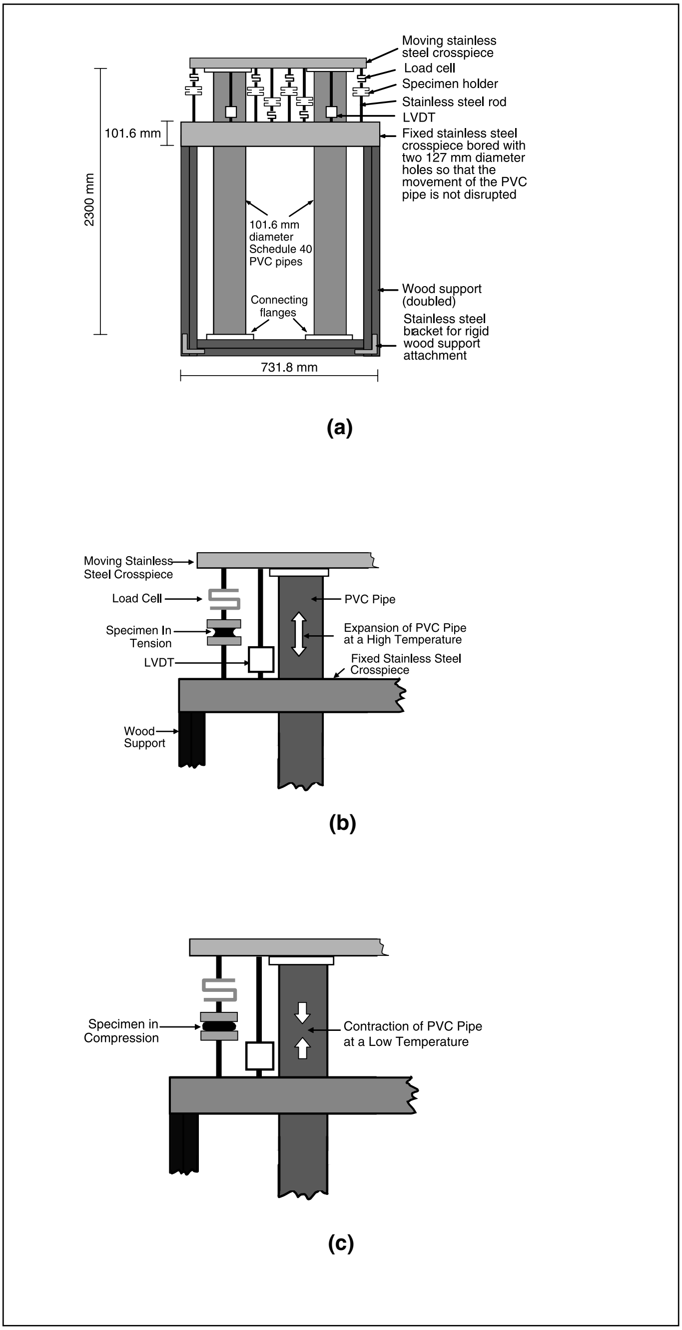

Figure 4—Schematic illustrations of (a) the thermally driven PVC engine, and the mechanism of the engine: (b) at a high temperature, the PVC pipe expands causing the specimen to be loaded in tension; and (c) at a low temperature, the pipe contracts causing the specimen to be loaded in compression.[15]

Cleveland, OH). A custom-written LabVIEW program was used to collect the voltage measurements from the Keithley system every 15 seconds, 24 hours a day. After one-minute worth of data was collected, the program averaged the values and appended the result to a tab-delimited database on a remote server. The engines allow changes in stiffness to be monitored as a function of exposure time.

RESULTS

Indoor Exposure

Figure 5 shows typical results for the two loading-unloading curves in the first characterization test on a specimen. The Mullins Effect is clearly present with higher stress levels during the first loading curve versus the second. Note that the unloading curves are the same in both cases. All subsequent loading-unloading curves will fall on top of the data in the second cycle.

Figure 6 shows a representative plot of changes in apparent moduli as a function of relaxation time for specimens under "static/hot/wet" conditions prior to exposure and after completion of fatigue deformation cycle. There were up to four replicates in each test, and the vertical bars indicate experimental uncertainty. Consequently, the difference seen between the two curves is significant. Note that there is no change in the curve shape, implying that time dependency of the apparent modulus is very similar before and after exposure. The magnitude of the apparent modulus, however, decreased significantly after exposure. Similar curves can be generated for all eight exposure conditions, but a plot with all 16 curves and their uncertainty is much cluttered. To facilitate comparison between different exposure conditions, stress relaxation data are presented as a fractional change in apparent modulus, F, as a function of relaxation time (see equation (3)). In such a graph, no change would be represented as a horizontal straight line at F=1.0. A horizontal line above or below F=1.0 indicates that exposure caused a vertical shift in the stress relaxation curve but no change in shape, i.e., the time dependence did not change. Something other than a horizontal straight line indicates a change in the

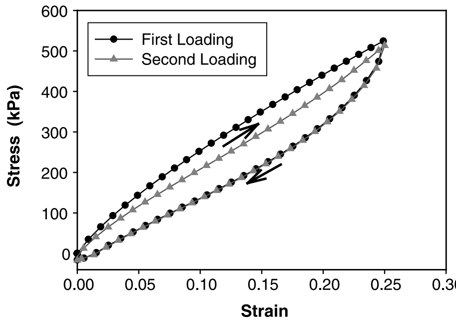

Figure 5—Loading-unloading curve for Mullins cycle.

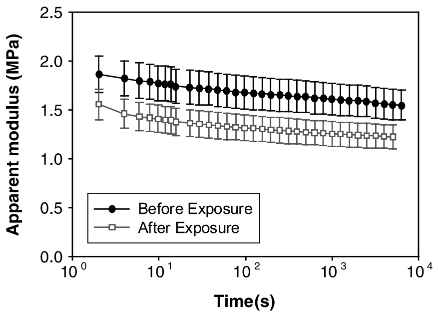

Figure 6—Variation of apparent modulus as a function of relaxation time for specimens under "static/hot/wet" conditions before and after exposures.

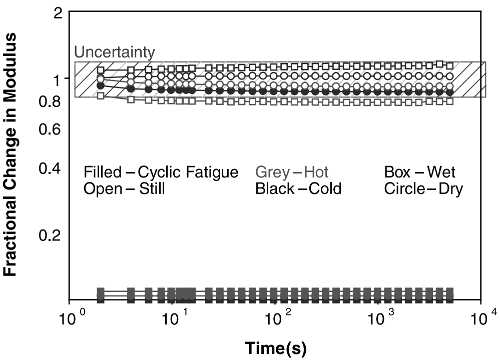

Figure 7—Stress relaxation curve for both static and cycle fatigue tests.

time dependence. The experimental uncertainty can be shown as a hashed region on each side of F=1.0 so if the point for a given curve falls within this region, there is no changes outside the experimental uncertainty. Stress relaxation data at different combinations of temperature and RH for static tests are shown in *Figure* 7. The lines at very low values of F indicate the samples have failed. The near straight lines parallel to the abscissa show that there is no change in the curve shape for all conditions.

The effect of temperature on the static performance of joints can be assessed by examining the conditions at the same RH, namely by comparing "static/cold/wet" with "static/ hot/wet," or "static/cold/dry" with "static/hot/dry." It is apparent that the temperature effect, either under a relatively dry or a moist environment, is insignificant. Also, moisture-induced deterioration in the static performance at a low temperature similarly seems unimportant, as revealed by comparing the "static/cold/dry" and "static/cold/wet" results. However, as shown in *Figure* 8, the combination of high temperature and RH produced a slight reduction in apparent modulus. All joints under static conditions remained intact and no joint failure was observed.

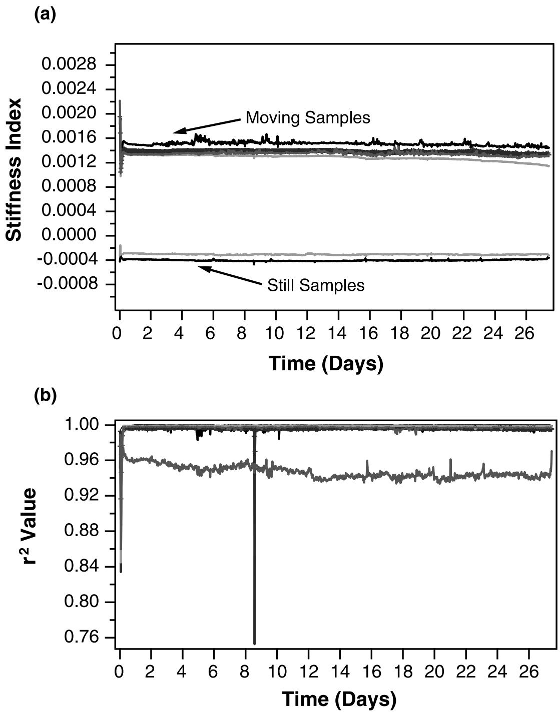

Figure 8—(a) Changes in stiffness index for samples with movement and no movement. (b) Corresponding squared correlation coefficients, r^2, as a function of exposure times in days for specimens under "fatigue/cold/dry" conditions. No visible failure is evident in the samples during the entire exposure.

Under cyclic fatigue deformation, the durability behavior differs considerably from that of static tests. The fractional changes in apparent modulus as a function of relaxation time for cyclic fatigue tests are included in *Figure* 7. In a "cold" and "dry" environment, the effect of fluctuating loads on the cyclic performance of sealant joints is insignificant. Furthermore, changes in the stiffness index of specimens, which were measured by the slopes of loading curves in the load-displacement plot for fatigue deformation cycle, were examined. The corresponding squared correlation coefficients, r^2, for the fitted slopes were also obtained to assess the goodness-of-fit of the slopes. The results for "fatigue/cold/ dry" are shown in *Figure* 8. The results for "static/cold/dry" are also included for comparison, but the slopes are always zero because there was no fatigue deformation cycle. In *Figure* 8a, the stiffness index of specimens under "fatigue/cold/dry" remained unchanged over a month of exposure, which agreed with the comparable stress relaxation data. The relative high values of corresponding squared correlation coefficients confirmed the reliability of the data obtained (see *Figure* 8b).

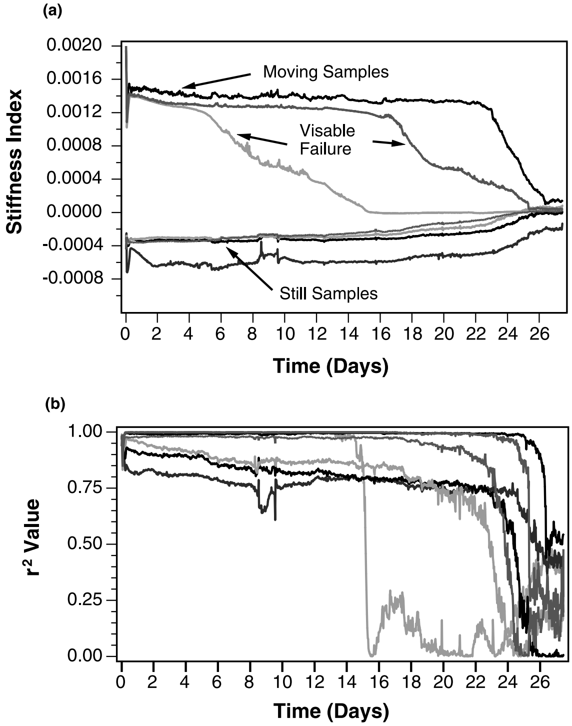

Figure 9—(a) Changes in stiffness index for both samples with movement and no movement. (b) Corresponding squared correlation coefficients, r^2, as a function of exposure times in days for specimens under "fatigue/hot/dry" conditions. Visible failure is evident in the three samples experiencing movement starting at eight days to 25 days.

However, as shown in *Figure* 7, the combination of cyclic fatigue with a high temperature, or with a high RH, or the combination of three aging factors, resulted in substantial changes in moduli. All joints tested under these conditions failed; thereby, the curves were plotted with ordinate magnitudes equal to zero. Changes in stiffness index and linear regression coefficients as a function of exposure time for "fatigue/ hot/dry" are shown in *Figure* 9. It can be seen that there was no change in stiffness index in early stages of exposure. With increasing exposure, the stiffness index decreased and was eventually followed by specimen failures. The stiffness index plots for "fatigue/cold/wet" and "fatigue/hot/wet" are shown in *Figures* 10 and 11, respectively. The stiffness for these specimens decreased drastically upon exposure, and then failures followed.

The loci of failure for all joints were visually observed as being cohesive within the sealant layers, indicating that the sealant itself was weak, while the interfacial adhesion between the sealant and the substrate was relatively robust. Further examination revealed

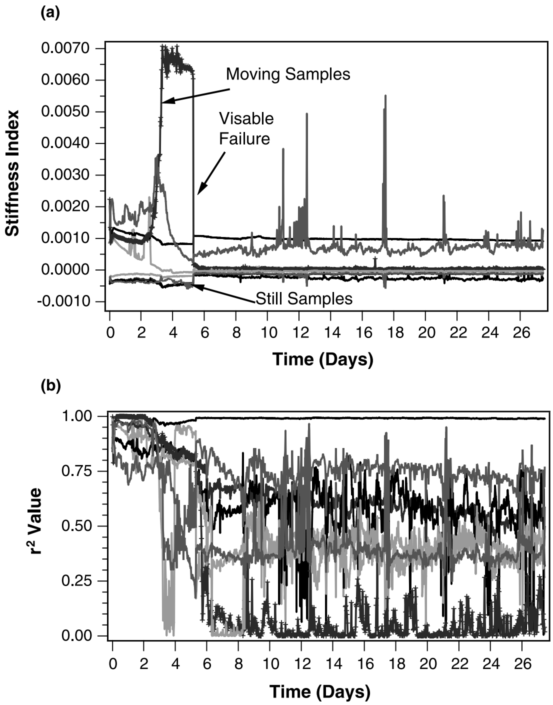

Figure 10—(a) Changes in stiffness index for both samples with movement and no movement. (b) Corresponding squared correlation coefficients, r^2, as a function of exposure time in days for specimens under "fatigue/cold/wet" conditions. Visible failure is evident in the samples at times less than six days.

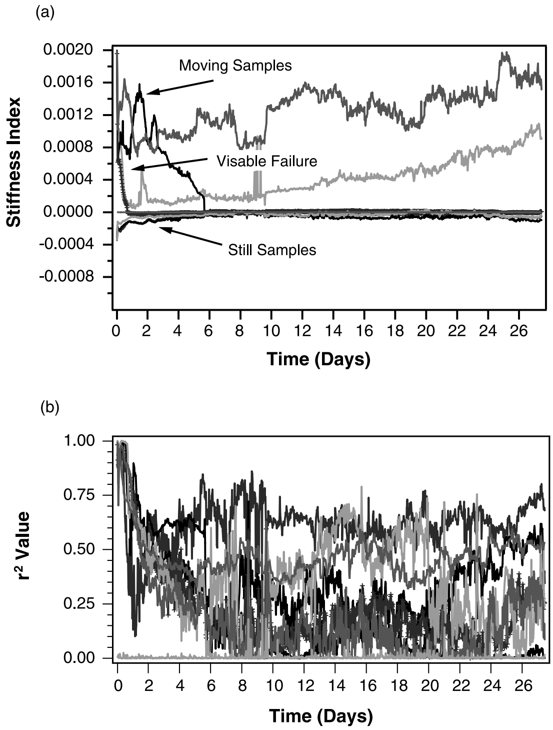

Figure 11—(a) Changes in stiffness index for both samples with movement and no movement. (b) Corresponding squared correlation coefficients, r^2, as a function of exposure times in days for specimens under "fatigue/hot/wet" conditions. Visible failure is evident in the samples at times less than two days.

extensive embrittlement. Therefore, it is highly likely that extensive crosslinking had taken place in the specimens, rendering them brittle and leading to premature failures. It is also clear that cyclic fatigue alone is not the critical factor leading to environmental failure of this sealant, but it is the combination of cyclic fatigue with other environmental factors (i.e., temperature or moisture) that is deleterious.

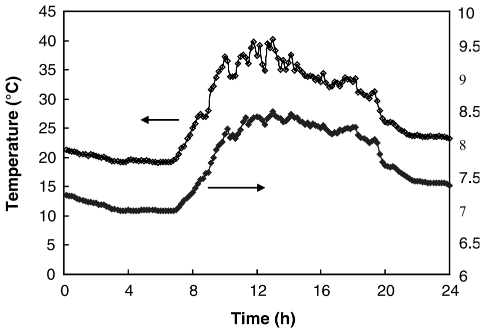

Figure 12—Variation of temperature of PVC pipe and the resulting displacement as a function of time. Measurements were made on July 1, 2004.

Field Exposure

In the case of field exposure, specimens were exposed to cyclic deformation induced by dimensional changes of PVC engines in which specimens were loaded in tension when outdoor air temperature was relatively high and in compression when the outdoor air temperature was relatively low. The evidence showing that changes in outdoor air temperature directly affect the magnitude of cyclic deformation imposed on specimens is shown in *Figure* 12. Because of temporal variations in outdoor air temperature, cyclic loading varies with the time of day. Such cyclic loading time series was what would be expected with sealants used in building structures. Load and displacement experienced by specimens were continuously monitored over one year, and the results are shown in *Figure* 13. In this plot, the data points on the right and left hand sides of the zero displacement line indicate which specimens were in tension and compression, respectively. For clarity, only data points collected over a day in each month were plotted. It should be noted, however, that data points for other days in the same month were very similar. From *Figure* 13, hysteresis in the load-displacement plot is clearly seen, demonstrating the viscoelastic nature of the sealant, which is common for all sealants although their observed degrees vary. It can

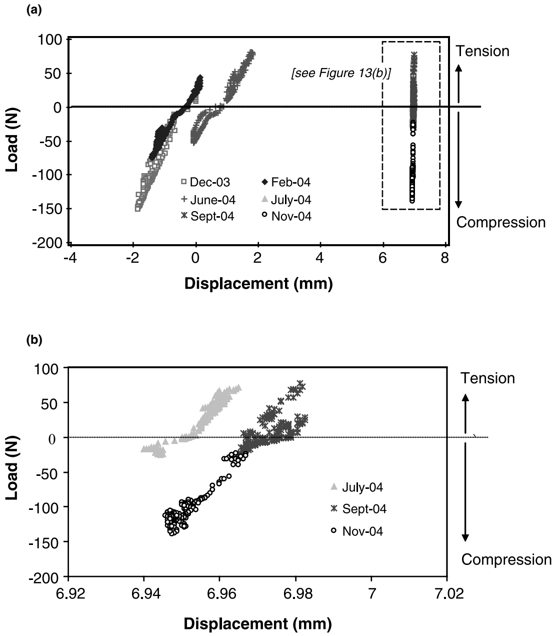

Figure 13—Load versus displacement recorded over one year of field exposure for displacement ranges of (a) –4 mm to 8 mm, and (b) 6.92 mm to 7.02 mm.

Table 1—Tabulation of Stiffness and the Corresponding Squared Correlation Coefficients, r^2, for Different Months of Exposure

Exposure Month	Stiffness (N/mm)	r^2 Coefficient
Dec. 2003	9.62	0.94
Feb. 2004	6.53	0.95
June 2004	5.98	0.97
July 2004	405.60	0.92
Sept. 2004	526.24	0.85
Nov. 2004	475.37	0.85

also be seen that specimens underwent both tensile and compressive loadings in December 2003 and February 2004, but compressive loading was found to be predominant. In contrary, specimens were mostly loaded in tension in June 2004, as shown by positive displacement values in the load-displacement plot. Interestingly, the displacement recorded in July 2004 differed significantly from that in June 2004, and the curve for July 2004 was located in the far right end of the plot, indicating that specimens had undergone a change from a mixture of compressive and tensile loading to a pure tensile loading. In later stages of exposure, specimens remained in tension.

Continuous monitoring of load and displacement allowed changes in stiffness to be examined, which was measured by the slopes of load-displacement plots (*Figure* 13). The values of stiffness are tabulated in *Table* 1, and squared correlation coefficients, r^2, for fitted curves are also included. It can be seen that r^2 value is relatively high for each month, signifying that each curve in the load-displacement plot can be fitted by a straight line with a highly reliable slope. From *Table* 1, it can be seen that the stiffness for freshly exposed specimens was 10 N/mm in December 2003. In the next seven months, the stiffness remained statistically unchanged, but in July 2004 the stiffness increased substantially to 400 N/mm. This significant increase in the stiffness shows that the sealants have undergone profound structural changes, and that summer exposure was more severe than winter exposure. Physical examination of the specimens revealed that the specimens had hardened considerably compared to unexposed specimens, indicating that extensive embrittlement had occurred. This observation indeed correlates well with the relatively high stiffness recorded. In later stages of exposure, the stiffness continued to increase to approximately 500 N/mm, and, eventually, the sealants failed cohesively.

DISCUSSION

Accurate prediction of in-service performance of sealants in less than real time has remained a modern unresolved scientific issue. At present, the generation of reliable performance data still requires long-term field exposure. Longer field exposure times are thought to reduce the risk of introducing a poorly performing product into the marketplace. However, the cost of developing new products is directly related to the product development time and the time-to-market. The more time in the pipeline, the more investment required and the smaller the eventual profit. Over the years, extensive efforts have been made to design a laboratory short-term test which provides an accurate indication of how well a building joint sealant will perform when exposed outdoors. However, these efforts have largely been unsuccessful, which arises mainly from the lack of success in relating field and laboratory results. From the results presented in this chapter, it is clearly seen that the current laboratory accelerated tests provide an excellent platform for evaluating the

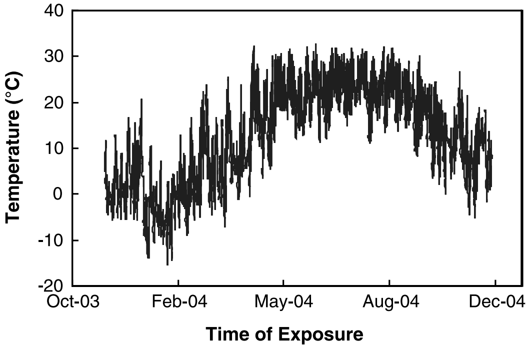

Figure 14—Changes in air temperature from December 2003 to November 2004.

service life of building joint sealants. Furthermore, the present tests were successful in duplicating the same failure mode that occurred in field exposure. Specifically, extensive crosslinking was found to occur in specimens under both field and laboratory accelerated exposures, which was eventually followed by brittle fracture. The current test method therefore circumvents the problems associated with accelerating the environmental attack with the use of unrealistically extreme doses of aging factors well above any likely seen in-service. Such tests often lead to unnatural failure mechanisms.

It is evident from the above discussion that the indoor laboratory accelerated test allows not only the individual effects of cyclic fatigue, temperature, and RH to be investigated independently, but also the synergistic effect of combining two or more factors. By using this test method, it has been shown that specimens were able to resist the individual influence of cyclic fatigue, high temperature, and RH, but degraded substantially when exposed to the combination of cyclic fatigue with a high temperature or RH, or the combination of these three factors. Fatigue, high temperature, and RH collectively provide strong synergism, thus accelerating the degradation mechanism and rapidly deteriorating sealant properties. Such observations correlated well with observations made under field exposure in that summer exposure was found to more aggressive in terms of environmental attack than winter exposure. This is because air temperature was generally higher in summer, as shown in *Figure* 14.

It is noteworthy that threshold type tests such as ASTM C719 have been widely adopted by the industry for selecting appropriate sealant formulations for specific applications. For example, ASTM C719 establishes the performance of sealants through the following protocol: a one-month period of static cure followed by a sequential stress regime including immersion in water (7 d), baking in an oven (7 d), exposure to UV, and, finally, mechanical cycling.[9] The samples are then visually evaluated for defects. Obviously, such a protocol assumes that no strong synergistic effect exists between the different aging factors. However, as shown by the present study, the effect of an individual factor acting alone may be different from the combined effect of two or more factors. The sealant material studied here will therefore pass ASTM C719, and, as such, will be mistakenly approved for installation on buildings, where it may fail prematurely. The existence of such synergistic effects raises serious concerns as to whether viewing the environmental effects of these factors independently is meaningful, highlighting the prime importance of accounting for such synergism in the development of scientifically meaningful accelerated durability tests.

CONCLUSIONS

A test methodology has been designed to duplicate the same failure modes occurring in in-service exposures. Such methodology employs a systematic approach in which both independent and synergistic effects of various aging factors on the durability of building joint sealants were evaluated in terms of changes in modulus, stiffness, and stress relaxation behaviors. Indoor accelerated exposures were carried out using an integrating sphere-based weathering chamber; while one-year field exposures were carried out in Gaithersburg, using a polyvinyl chloride (PVC) device, which relied on thermal response of PVC to outdoor air temperature to induce cyclic fatigue deformation on sealants. Indoor test results revealed that cyclic fatigue, high temperature, or moisture, on sealant mechanical properties acting alone did not degrade this sealant, in combination, however (e.g., cyclic fatigue deformation with temperature and/or moisture) was detrimental, resulting in extensive embrittlement and leading to premature failure. Sealants exposed to field conditions exhibited the same behavior, indicating that the accelerated test methodology provided an accurate indication of the durability of sealants exposed outdoors. The present study has clearly shown the importance of designing experiments that enable effects of various aging factors to be systematically evaluated, with test results correlating to field performance if accelerated conditions more accurately reflect the balance of field exposure conditions.

References

(1) Tan, K.T., White, C.C., Benatti, D.J., Stanley, D., and Hunston, D.L., in *Handbook of Sealant Technology*, Mittal, K.L. and Pizzi, A. (Eds.), in press.

(2) Wolf, A.T., in *Durability of Building Sealants*, Beech, J.C. and Wolf , A.T. (Eds.), p. 63-89, E & FN Spon, London, UK, 1996.

(3) Lacher, S., Williams, R.S., Halpin, C., and White, C.C., in *Service Life Prediction: Challenging the Status Quo*, Martin, J.W., Ryntz, R.A., and Dickie, R.A. (Eds.), Federation of Societies for Coatings Technology, Blue Bell, PA, p. 207, 2004.

(4) Lowe, G.B., in *Durability of Building Sealants*, Wolf, A.T. (Ed.), p. 225-234, RILEM Publications S.A.R.L., Cachan Cedex, France, 1999.

(5) Woolman, R. and Hutchinson, A., *Resealing of Buildings: A Guide to Good Practice*, Butterworth-Heinemann, Oxford, UK, 1994.

(6) Grunau, E., *Service Life of Sealants in Building Construction* (in German), Research Report, Federal Ministry for Regional Planning, Building and Urban Planning, Bonn, Germany, 1976.

(7) Chiba, R., Wakimoto, H., Kadono, F., Koji, H., Karimori, M., Hirano, E., Amaya, T., Sasatani, D., and Hosokawa, K., *Improvement System of Waterproofing by Sealants*, p. 175-199, Japan Sealant Industry Association, Tokyo, Japan, 1992.

(8) Expenditures for Residential Improvements and Repairs—1st Quarter, Current Construction Reports, U.S. Census Bureau, Department of Commerce, Washington, D.C., 2002.

(9) ASTM C719-93 (2005), "Standard Test Method for Adhesion and Cohesion of Elastomeric Joint Sealants Under Cyclic Movement (Hockman Cycle)," American Society for Testing and Materials, Philadelphia, 1993.

(10) White, C.C., Tan, K.T., Hunston, D.L., Hettenhouser, J., and Garver, J.D., in *Service Life Prediction for Sealants Phase II Report: Precision Exposure Chambers and Screening Experiments*, White, C.C. (Ed.), p. 10-37, NIST, Gaithersburg, MD, 2007.

(11) Chin, J.W., Byrd, E., Embree, N., Garver, J., Dickens, B., Finn, T., and Martin, J., *Rev. Sci. Instrum.*, 75 (11), 4951 (2004).

(12) Taylor, C.R., Greco, R., Kramer, O., and Ferry, J.D., *Trans. Soc. Rheol.*, 20, 141 (1976).

(13) Ferry, J.D., *Viscoelastic Properties of Polymers*, John Wiley & Sons, Inc., 3rd Ed., New York, 1980.

(14) Ketcham, S.A., Niemiec, J.M., and McKenna, G.B., *J. Eng. Mech.*, 669 (1996).

(15) White, C.C., Tan, K.T., O'Brien, E.P., Hunston, D.L., and Williams, R.S., in *Service Life Prediction for Sealants Phase II Report: Precision Exposure Chambers and Screening Experiments*, White, C.C. (Ed.), p. 38-72, NIST, Gaithersburg, MD, 2007.